HHS Public Access

Author manuscript

J Comp Neurol. Author manuscript; available in PMC 2020 January 01.

Published in final edited form as:

J Comp Neurol. 2019 January 01; 527(1): 259–269. doi:10.1002/cne.24457.

Sub-topographic maps for regionally enhanced analysis of visual space in the mouse retina

Rana N. El-Danaf[1] and **Andrew D. Huberman**[*,1,2,3,4]

[1]Department of Neurobiology, Stanford University School of Medicine, Stanford, California, USA

[2]Department of Ophthalmology, Stanford University School of Medicine, Stanford, California, USA

[3]Stanford Neurosciences Institute, Stanford University School of Medicine, Stanford, California, USA

[4]BioX, Stanford University School of Medicine, Stanford, California, USA.

Abstract

In many species, neurons are unevenly distributed across the retina, leading to nonuniform analysis of specific visual features at certain locations in visual space. In recent years, the mouse has emerged as a premiere model for probing visual system function, development and disease. Thus, achieving a detailed understanding of mouse visual circuit architecture is of paramount importance. The general belief is that mice possess a relatively even topographic distribution of retinal ganglion cells (RGCs)- the output neurons of the eye. However, mouse RGCs include ~30 subtypes; each responds best to a specific feature in the visual scene and conveys that information to central targets. Given the crucial role of RGCs and the prominence of the mouse as a model, we asked how different RGC subtypes are distributed across the retina. We targeted and filled individual fluorescently tagged RGC subtypes from across the retinal surface and evaluated the dendritic arbor extent and soma size of each cell according to its specific retinotopic position. Three prominent RGC subtypes: On-Off direction selective RGCs, object-motion-sensitive RGCs, and a specialized subclass of non-image-forming RGCs each had marked topographic variations in their dendritic arbor sizes. Moreover, the pattern of variation was distinct for each RGC subtype. Thus, there is increasing evidence that the mouse retina encodes visual space in a region-specific manner. As a consequence, some visual features are sampled far more densely at certain retinal locations than others. These findings have implications for central visual processing, perception and behavior in this prominent model species.

Graphical Abstract

[*]correspondence: adh1@stanford.edu.

Conflict of interest statement

The authors declare no conflict of interest.

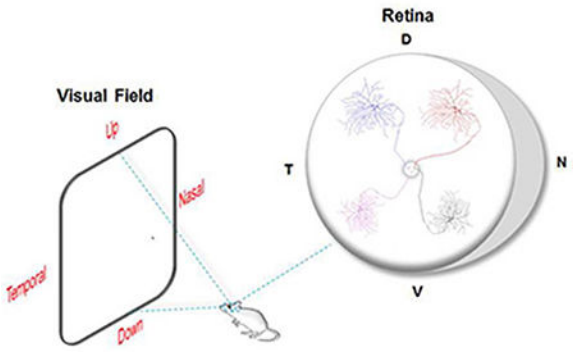

All visual information is processed through the activity of various subtypes of retinal ganglion cells (RGCs). As a prominent model for studying the visual system, the mouse retina was thought to encode visual space in a uniform manner. Here, we discovered that three morphologically and functionally distinct subtypes of RGCs show distinct retinotopic organizations. Therefore, signals located in different portions of the visual space are conveyed and analyzed differently in the brain.

Keywords

Retina; Retinal ganglion cells; Vision; Topography; Glaucoma; Retinofugal

1. Introduction

Visual processing begins in the retina. Specialized regions of the subcortical and cortical brain then analyze retinal information and integrate it with processing of other modalities such as audition, emotional state and motor circuitry to generate percepts and behaviors. The amount and quality of visual information that reaches the brain is bottlenecked by the number, function and distribution of retinal neurons, in particular the retinal ganglion cells (RGCs) - the output neurons of the eye. RGCs include ~30 subtypes, each having distinct morphological and functional characteristic, and responding best to a particular feature in the visual world (Baden et al., 2016; Dhande et al., 2015). In other words, each RGC subtype can be thought of as a unique channel of visual information for the brain. Understanding how as a total population and as distinct subtypes, RGCs are topographically organized (i.e. in respect to their exact position within the retina) is thus essential to understanding how different aspects of the visual world are conveyed to and analyzed in the brain.

A salient example of how variation in RGC density impacts the structure and functional output of central visual processing is the fovea. The foveal region of the primate retina contains RGCs at much greater density and decreased dendritic size compared to the retinal periphery, which allows this region to sample visual space at a much finer scale (Dacey and Petersen, 1992; Dacey, 1993; Yamada et al., 1996; Gomes et al., 2005).

In recent years, the mouse has emerged as a premiere model for studying various aspects of visual system development, function and disease at the retinal, subcortical, cortical and behavioral level (reviewed in: Seabrook et al., 2017). Previous studies described relatively

flat distributions in RGC density across the retina when compared to other animals, as well as little or no correlation in soma or dendritic size with eccentricity (Dräger and Olsen, 1981; Jeon et al., 1998; Sun et al., 2002; Coombs et al., 2006). Given that previous studies focused on RGC topography in the mouse lumped all RGCs together as a single group, there remains the very possibility that the mouse retina may in fact harbor regions in which specific RGC types vary their density across the retinotopic surface, and therefore sample the environment differently for specific visual features according to retinal location. Indeed, a recent study from Wong and coworkers found that two types of alpha RGCs, sustained On-alpha RGCs (sOn-α) and sustained Off-alpha RGCs (sOff-α), exhibit regional variations in their density and dendritic arbor sizes along the nasal-temporal (N-T) axis (Bleckert et al., 2014). This presumably is to allow enhanced sampling of motion in the binocular visual field. An important set of unresolved questions now face the field:

- **i.** Are alpha RGCs the exception or do other RGC subtypes vary their density by topographic position in the mouse?
- **ii.** If so, along what retinal axes do those variations occur?
- **iii.** How do such topographical variations impact central processing?

Here we asked whether RGCs vary their features so as to create specialized sub-topographical maps in the mouse retina. We explored this in mice using tools where somal and dendritic parameters can be studied. By examining these features in four transgenically labeled RGC subtypes, we obtained detailed analysis of how the characteristics of individual RGC subtypes vary as a function of precise retinal location (Osterhout et al., 2011; Rivlin-Etzion et al., 2011; Zhang et al., 2012). Our results are surprising: several RGCs that perform specific processing roles and that project into the retino-geniculo-cortical pathway as well as other perceptually- and behaviorally-relevant targets, show marked variation according to topographic location.

Remarkably, each of these RGC subtypes also had a different topographical pattern: dendritic size variations occurred along several retinal axes, distinct from the one previously described for alpha RGCs by Bleckert et al. (2014). These findings confirm and add to the growing evidence that mouse visual system is not as simple as previously thought, they highlight as well the functional relevance of specific RGC subtypes for central visual processing and behavioral output.

2. Materials and Methods

2.1 Mice

Adult mice ranging in age between postnatal days (P) 30–60, of either sex were used. Three different transgenic mouse lines were used to target specific fluorescently-labeled RGC subtypes (Figures 1A,2): thyrotropin-releasing hormone receptor-EGFP mice (TRHR-GFP; Rivlin-Etzion et al., 2011; Osterhout et al., 2014; Stafford et al., 2014; Bickford et al., 2015); Cadherin-3-EGFP mice (Cdh3-GFP; Osterhout et al., 2011; Osterhout et al., 2014) and TYW3 (Kim et al., 2010; Zhang et al., 2012). All experimental procedures were approved by the Institutional Animal Care and Use Committee at Stanford University School of Medicine.

2.2 Cell fills

Labeling of individual RGCs was performed using a previously described protocol (Beier et al., 2013; Dhande et al., 2013: Cruz-Martin et al., 2014; El-Danaf and Huberman, 2015). Mice were anesthetized with inhalant isoflurane and the eyes were enucleated. The dorsal pole of the left and right eyes were marked before removing them from the animal, using waterproof color markers thus ensuring that knowledge about retinal location was preserved (Wei et al., 2010). Retinas were cut in half along the dorsal-ventral (D-V) or nasal-temporal (NT) axes using vascular landmarks (Wei et al., 2010), and kept in oxygenated (95% O_2/5% CO_2) $NaHCO_3$ (23 mM) containing Ame's medium (Sigma-Aldrich, catalog #A1420). The fluorescent RGC somas were localized using differential interference contrast (DIC) and epifuorescence microscopy. RGCs were targeted with borosilicate glass electrodes (Sutter Instruments; 15–20 MΩ) containing Alexa Fluor 555 hydrizide dye (10 mM in 200 mM KCl; Invitrogen, catalog #A20501MP), and were completely filled by applying hyperpolarizing current pulses ranging between 0.1– 0.9 nA for ≤1 minute.

2.3 Retinal histology

Immunohistochemical staining for amacrine-cell stratification landmarks was performed as described previously (Dhande et al., 2013; El-Danaf and Huberman, 2015). Immediately after cell filling, retinas were fixed at room temperature with 4% paraformaldehyde (PFA) for 1h. They were then washed in 1X PBS (3x, 20 mins each) and incubated in blocking solution (10% donkey serum with 0.25% Triton-X) for 1 h at room temperature. The retinas were then incubated for 4–6 days at 4°C in blocking solution containing primary antibodies: rabbit anti-GFP (1:1000; Invitrogen, catalog #A6455; Research Resource Identifier (RRID): AB_221570], guinea pig anti-VAChT (1:500; Millipore, catalog #AB1588; RRID: AB_2187981), and goat anti-ChAT (1:100; Millipore, catalog#AB144P; RRID: AB_2079751). Retinas were rinsed with PBS (4x, 30 minutes each), and incubated overnight at 4°C in the following secondary antibodies: Alexa Fluor 488 donkey anti-rabbit (1:1000; Invitrogen, catalog #A21206; RRID: AB_141708), Alexa Fluor 647 donkey anti-guinea pig (1:500; Jackson Immuno Research, catalog #706-606-148), and Alexa Fluor 647 donkey anti-goat (1:500; Life Technologies, catalog #A21447; RRID: AB_10584487). Retinas were then rinsed in PBS at room temperature (2–3 hours, 30-minute cycles), and coverslipped with Vectashield containing DAPI to label cell nuclei (Vector Laboratories, catalog# H-1200, RRID: AB_2336790). Spacers made of tape were placed between the slides to avoid retinal tissue compression.

2.4 Imaging

Protocols were previously described (El-Danaf and Huberman, 2015). Briefly, coverslipped retinas/RGCs were imaged using a laser scanning confocal microscope (Zeiss LSM 710) and 40X water immersion objective lens (LDC-Apochromat 40x/1.1). Z-stacks were collected at a scanning resolution of 1024×1024 pixels with a 0.5 μm Z-step increment size, and a Kalman averaging of 2–4. To obtain the location of individual RGCs, images of the retinal halves were acquired at 5X using an epifluorescence microscope (Zeiss Axio Imager 2) equipped with an Axiocam HR camera, and were later stitched together into whole-retina, orientationpreserved images, using Adobe Photoshop software.

2.5 Analysis

A total of 296 intracellularly labeled RGCs were analyzed using Fiji software to track their location and to obtain morphological measurements of their somal and dendritic properties. The height and width of each retina was normalized between different mice to control for possible variations in size. The location of each individually labelled RGC was recorded in Fiji as a coordinate value by marking their position with respect to the optic nerve head (ONH) and the outer boundaries of the retina, keeping track of D-V and N-T orientations (e.g.: ONH: 0, 0; periphery: −1,1; Y-axis= D-V axis; X-axis = N-T axis) (see Figures 3A, 4A, 5A).

Soma and dendritic diameters were obtained from the maximum intensity projections of Zstacked images. Dendritic diameter was calculated as described in: (Bleckert et al., 2014), where the 2D polygonal area of each dendritic arbor was measured by outlining the outermost dendritic processes of each RGC, and the value reported is the diameter of a circle that was equal to it. Data shown represent soma and dendritic diameters as a function of eccentricity (the absolute distance of each RGC from the ONH), as a function of percent distance along the N-T axis (X-axis coordinates of each RGC converted into a percent number where peripheral Nasal = 0% and peripheral Temporal = 100%), and as a function of percent distance along the D-V axis (Y-axis coordinate of each RGC converted into a percent number where peripheral Ventral = 0% and peripheral Dorsal = 100%).

Statistical analyses were reported by fitting the data points to a linear regression, and significance of $r^2 \geq 0.5$ was chosen.

3. Results

For this study, we used three transgenic mouse lines that collectively label 4 distinct RGC subtypes with fluorescent proteins (Green: GFP; or yellow: YFP). The mouse lines we employed and the RGC subtypes they label were as follows: TRHR-GFP mice/ posterior tuned On-Off direction selective RGCs (pOn-Off DSGCs) (Rivlin-Etzion et al., 2011; Osterhout et al., 2014). Cdh3-GFP mice/non-image forming “On” (NIF-On) and non-image forming “diving” (NIF-diving) RGCs labelled (Osterhout et al., 2011; 2014); TYW3 mice/W3-RGCs (Kim et al., 2010; Zhang et al., 2012) (Figures 1A, 2). The overall GFP/YFP expression patterns in the retinas of these mice have been previously shown (Kim et al., 2010; Rivlin-Etzion et al., 2011; Osterhout et al., 2011; Zhang et al., 2012; Osterhoust et al., 2014), and it is important to note that it might not reflect the actual distribution of these RGCs. Due to transgene effects, the full population of these different RGC subtypes might not be represented. Here, we used the GFP/YFP expression as a tool to target and label these distinct subtypes of RGCs. Our goal was to identify possible topographical variations in dendritic and soma size for each subtype in terms of eccentricity and location along the different retinal axes. The rationale for this is that each portion of the retina views a different portion of visual space and communicates that to distinct subcortical targets and portions of targets (Figures 1B, C). As noted above, the retinotopic organization of all RGCs collectively in the mouse, is known (Jeon et al., 1998), but there is reason to think that some RGC subtypes might vary their density and dendritic extent and thus spatial aspects of their receptive field properties, within that overall distribution (Bleckert et al., 2014). We

therefore targeted individual GFP+ or YFP+ somas in each of the three mouse lines described above, and filled them with Alexa 555 (red) to reveal their dendritic morphology and stained the retinas for the enzyme Choline Acetyltransferase (ChAT) the rate limiting enzyme for Acetyl Choline production (Fig. 2). Within the retina, ChAT is enriched in On and in Off starbust amacrine cells, whose processes act as fiduciary markers for the Off and On sublaminae of the inner plexiform retinal layer (IPL). Figure 2 shows the different expression patterns of GFP (Figures 2A,D,G) and YFP (Figure 2J) in the transgenic retinas, individual GFP/YFP RGCs after filling when viewed *en face* (Figure 2B,E,H,K), as well as from the side view (Figure 2C,F,I,L) which reveals their stratification relative to the On and Off ChAT processes.

3.1 pOn-Off DSGCs display dendritic field differences along the dorsal-ventral axis

We first examined the pOn-Off DSGCs (*n=105* RGCs) labeled in TRHR-GFP transgenic mice (*N=16* mice). These cells are characterized with looping arbors that co-stratify with the two ChAT bands in the inner plexiform layer (IPL; Figures 2A-C; Figure 3; Rivlin-Etzion et al., 2011). Analyzing the soma diameters of individually labelled RGCs revealed no significant changes along any of the position parameters that we examined (Eccentricity from ONH: Figure 3F, $r^2 = 0.1537$; % distance N-T axis: Figure 3G, $r^2 = 0.0006$; % distance D-V axis: Fig. 3H, $r^2 = 0.0968$). Additionally, there were no significant changes in dendritic diameter as a function of eccentricity from ONH (Figure 3I, linear regression $r^2 = 0.2899$), nor along the N-T axis (Figure 3J, linear regression $r^2 = 0.0035$). By contrast, dendritic diameter analysis revealed that these RGCs display D-V differences in their size. There is roughly a 1.7fold increase in dendritic field size of dorsally vs. ventrally located RGCs (Figure 3K; linear regression $r^2 = 0.5648$). Figures 3B-E show different examples of pOn-Off DSGCs labelled from the dorsal and ventral regions of the retina revealing these dendritic arbor size differences. These results reveal that these pOn-Off DSGCs sample visual space differently along the V-D axis, indicating perhaps a higher resolution sampling of signals situated in the upper visual field. It is important to note that the organization of TRHR-GFP RGC dendrites is different than that of the overall uniform cell density reported in the dopamine receptor-4 (DRD4-GFP) transgenic mouse line (Huberman et al., 2009; Bleckert et al., 2014). . This is likely because these 2 transgenic mouse lines label distinct populations of the posterior tuned direction selective RGCs (Huberman et al., 2009; Rivlin-Etzion et al., 2011).

3.2 NIF-On RGCs display changes in dendritic field size along the nasal-temporal axis

In the Cdh3-GFP transgenic mice, RGCs expressing GFP comprise two subtypes that project to non-image forming visual targets in the brain (Osterhout et al., 2011). These two subtypes differ in their *en face* morphology as well as their stratification patterns in the IPL (Figures 2D-I; Osterhout et al., 2011). The “On” subtype have mono-stratified dendritic arbors that terminate right below the On-ChAT band (Figures 2D-F; Osterhout et al., 2011); while the “diving” subtype are bistratified with arbors that “dive” above and below the two ChAT bands (Figures 2G-I;Osterhout et al., 2011). We labeled a total of 100 RGCs in the Cdh3-mice (Figure 4; *N=10* mice; *n=44* NIF-On RGCs; *n=56* NIF-diving RGCs), and traced their location (Figure 4A). It’s important to note that GFP expression in this particular mouse line is absent in the upper part of the dorsal retina, which is also reflected in our data (Fig. 4A;

Osterhout et al., 2011). It is yet to be determined whether this expression pattern is simply a result of the transgene or whether it's due to the lack of these RGC subtypes in this region.

We examined soma diameter of both subtypes and found no significant differences relative to retinal location (data not shown). Further dendritic arbor size analysis revealed that the NIF-On RGC subtype display variability along the N-T axis, where temporally located RGCs show a ~1.8fold increase in dendritic field size (Fig. 4G; linear regression $r^2 = 0.5822$), compared to other locations (Eccentricity from ONH: Figure 4F, $r^2 = 0.00001$; % distance V-D axis: Figure 4H, $r^2 = 0.0198$). This is further displayed in the cell fills shown in figures 4B-C where the nasally located RGCs have a much smaller dendritic arbor size compared to the temporally located one. By contrast, the NIF-diving RGCs do not show significant changes relative to their retinal location (Figure 4D-E; Eccentricity from ONH: Figure 4I, $r^2 = 0.0035$; % distance N-T axis: Figure 4J, $r^2 = 0.0156$; % distance V-D axis: Figure 4K, $r^2 = 0.0007$).

3.3 W3-RGCs display changes in dendritic field as a function of eccentricity

Lastly we analyzed W3 RGCs ($n=91$ RGCs), the brightly YFP-expressing ganglion cells in the TYW3 transgenic mouse line ($N=13$ mice; Kim et al., 2010; Zhang et al., 2012). These neurons comprise the most abundant as well as one of the smallest RGC subtypes in the murine retina (Figure 2J-L; Zhang et al., 2012). They have one thick dendritic arbor that stratifies between the two ChAT bands, as well as some dendritic sprouts that terminate at the boundary of the inner nuclear layer (INL; Figure 2L; Zhang et al., 2012). By examining the soma diameter of the dye filled W3-RGCs across different locations (Figure 5A), we found no significant correlations as function of eccentricity from ONH (Figure 5F, $r^2 = 0.06482$), % distance N-T axis (Figure 5G, $r^2 = 0.1\times10^{-6}$), or % distance V-D axis (Figure 5H, $r^2 = 4.8\times10^{-5}$). Similarly, no linear correlations were found when examining dendritic size as a function of % distance along the N-T axis (Figure 5J, $r^2 = 0.01747$) nor along the V-D axis (Figure 5K, $r^2 = 0.0467$). However, we found a relationship between dendritic arbor diameter and eccentricity. There was approximately a 2fold change in dendritic size, where W3 RGCs located closer to the ONH were significantly smaller than those situated at the periphery (Figure 5I; linear regression $r^2 = 0.5356$). Examples of dye filled W3-RGCs shown in Figures 5B-E reveal these differences. These results are consistent with the density measurements published previously by Zhang et al., 2012, where it was reported that W3-RGCs' density is lower in the peripheral compared to the inner retina.

4. Discussion

Our results provide further support for the idea that visual space is sampled non-uniformly by the mouse retina. We discovered that three out of the four RGC subtypes that we examined exhibited topographical arrangements in the retina and each of those was distinct from the other: pOn-Off RGCs (TRHR-GFP) displayed smaller dendritic fields in the ventral retina, while smaller NIF-On RGCs (Cdh3-GFP) were present in the nasal retina and W3-RGCs (TYW3) showed eccentricity related changes in their dendritic field size (Figure 6A-D). Both of this current study and that of Bleckert et al., 2014 included On-stratifying RGCs (sOn-α RGC and NIF-On RGC) which showed retinotopic differences along the N-T axis.

However, the changes observed, were along opposite axes: the sOn-α RGCs were larger in the nasal retina, whereas the NIF-On RGCs were larger in the temporal side. Furthermore, both studies showed that certain RGC subtypes do not display any significant changes in their size or density across the retina, and these include the NIF-diving RGCs and the transient Off-alpha RGCs, respectively (Bleckert et al., 2014). These results indicate that topographical arrangement could be a consequence of the functional and structural variations inherent to these different RGC subtypes.

Previous studies in mouse failed to reveal prominent location-dependent changes in RGC dendritic arbor size, likely because they treated all RGCs as a single group, or classified them in into broad categories by virtue of their soma sizes (Drager and Olsen, 1981; Jeon et al., 1998; Sun et al., 2002). Those findings, paired with the understanding that the overall acuity of the mouse visual system is relatively low compared to other model species such as cats and primates suggested that the entire mouse retina is more or less like the peripheral retina of the primate-low resolution- and thus mice may not rely on their visual system much at all under natural conditions (reviewed in: Huberman and Niell, 2011; Baker at al., 2013). However, emerging studies reveal that the mouse visual system is not as simple as previously thought. Furthermore, recent work shows that at the behavioral level, mice respond robustly to stimuli presented in specific portions of the visual field (Yilmaz and Meister, 2013; Wei et al., 2015), and that many higher cortical areas are ‘tuned’ to detect specific visual features in designated visual field locations (Marshel et al., 2011).

4.1 Functional relevance of RGC’s topographical arrangement

The presence of sub-topographical regions in the retina might be essential for dictating various behavioral aspects of survival for this species, such as foraging for food, detection of predators or prey, etc. (Figure 6E). Each of the RGCs studied here is essential for detecting a specific feature in the visual space including object motion and direction. We found that pOn-Off DSGCs have reduced dendritic arbor size in the ventral retina. This region is essential for sampling elements that are located in the upper visual field. Consequently, the organization of these neurons might provide mice with a greater resolution for detecting overhead objects moving in the posterior direction, such as a hawk looming in from the front and above the mouse (Figure 6E). This particular visual stimulus has been shown to elicit specific, robust behaviors in mice such as freezing and fleeing (Yilmaz and Meister, 2013). Similarly, the presence of smaller NIF-On RGCs (Cdh3-GFP) in the nasal retina is perhaps crucial for enhanced discrimination of signals located in the peripheral visual space, for example a cat stalking the mouse from the side (Figure 6E). The W3-RGCs eccentricity gradient is arranged to enhance fine-scale analysis of stimuli in the central visual field, such a snake attacking from the front or recognition of a conspecific (Figure 6E).

These specialized retinal arrangements might have been an adaptation to accommodate this species to its environmental niche, comparable to the importance of the fovea for resolving images in humans and primates. Indeed, the vastly expanded portion of the primate cortex that underlies foveal processing, and the reliance on foveal vision for analysis of fine spatial detail underscores the significance of the RGC-to-central processing relationship (Tootell et al., 1988; Muller et al., 2016). A similar degree of central-versus-peripheral scaling is

observed for the “area centralis” of the carnivore retina (Peichl, 1992; Mowat et al., 2008) and the ‘visual streak’ in the rabbit- an elongated portion of the retina containing a relatively greater number of RGCs for enhanced acuity to view the horizon and detect the presence and approach of potential predators (Davis, 1929: Oyster et al., 1981). Indeed, there is a fairly large body of classic work that describes the many unique and adaptively optimized RGC topographic variations that exist in the animal kingdom, where the RGC topography is directly related to the visual requirements, ecological habitats, predatory and foraging behaviors of different species. For example, there is the mixed fovea/streak arrangement present in certain diving birds - with the streak for higher acuity viewing of the horizon and the fovea for spotting fish swimming below the ocean’s surface (Hayes et al., 1991) or the “J” shaped fovea found in elephants to view locations specifically within the arced trajectory of the animal’s trunk during reaching (Stone and Halasz, 1989; Pettigrew et al., 2010). Other examples of specialized retinal organizations have also been previously reported in: birds (Inzunza et al., 1991; Coimbra et al., 2009), sharks (Lisney and Collin, 2008), penguins (Coimbra et al., 2012), lizards (Fite and Lister, 1981), and giraffes (Coimbra et al., 2013), among others. The above examples illustrate the adaptive and primary utility of the visual system for each of those species.

4.2 Consequences for degeneration and disease

RGC loss has been implicated in various neurodegenerative disorders (Jindal, 2015). In many cases, RGC death is shown to occur non-uniformly across the retina. For example, in human glaucoma patients, certain patterns of visual field defects are monitored and studied to detect the emergence and progression of this widespread blinding disease (Stewart et al., 1991; Kitazawa et al., 1997). Moreover, in the DBA/2J glaucoma mouse model, degeneration ensues in a fanshaped sectorial pattern (Jakobs et al., 2005). This uneven degradation is present in other retinal diseases as well, such as Retinitis pigmentosa, where RGCs’ changes in the central region are more prominent that those found in the peripheral retina (Anderson et al., 2016). These topographical patterns of degeneration may be the result of subtype-specific vulnerability of RGCs to different insults or diseases. Indeed, this was shown in several glaucoma models, where Off-stratifying RGCs were found to be especially susceptible to death following ocular hypertension (Della Santina et al., 2014; El-Danaf and Huberman, 2015; Ou et al., 2016). Our findings of the presence of sub-topographical maps in the mouse retina might shed some light into understanding some of these topographically-related changes in various retinal diseases, in the hopes of discovering therapies that target those specific RGC subtypes.

Acknowledgements

We would like to thank Dr. Rachel Wong, Dr. Wan-Qing Yu, Dr. Tania Seabrook and Dr. Onkar Dhande for helpful comments on an earlier version of this manuscript. We also thank Dr. Ben Stafford for advice on data analysis and Dr. Markus Meister for contribution of the TYW3 mouse line. R. E.-D. carried out all the experiments and data analysis. R. E.-D. and A.D.H designed the study and wrote the paper. This work was supported by NIH RO1 EY022157 (A.D.H.), the Catalyst for a Cure Initiative from the Glaucoma Research Foundation, a grant from the Pew Charitable Trusts (A.D.H.), and by NIH U01 NS090562.

References

Anderson E, Greferath U, & Fletcher L (2016). Changes in morphology of retinal ganglion cells with eccentricity in retinal degeneration. Cell Tissue Research, 364(2):263–71. [PubMed: 26670589]

Baden T, Berens P, Franke K, Román Rosón M, Bethge M, & Euler T (2016). The functional diversity of retinal ganglion cells in the mouse. Nature, 529(7586):345–50. [PubMed: 26735013]

Beier T, Borghuis G, El-Danaf R, Huberman A, Demb J, & Cepko C (2013). Transsynaptic tracing with vesicular stomatitis virus reveals novel retinal circuitry. Journal of Neuroscience, 33(1):35–51. [PubMed: 23283320]

Bickford M, Zhou N, Krahe T, Govindaiah G, & Guido W (2015). Retinal and Tectal "DriverLike" Inputs Converge in the Shell of the Mouse Dorsal Lateral Geniculate Nucleus. Journal of Neuroscience, 35(29):10523–34. [PubMed: 26203147]

Bleckert A, Schwartz G, Turner M, Rieke F, & Wong R (2014). Visual space is represented by nonmatching topographies of distinct mouse retinal ganglion cell types. Current Biology, 24(3): 310–5. [PubMed: 24440397]

Coombs J, van der List D, Wang G, & Chalupa L (2006). Morphological properties of mouse retinal ganglion cells. Neuroscience, 140(1):123–36. [PubMed: 16626866]

Coimbra J Trévia N, Marceliano M, da Silveira Andrade-Da-Costa B, Picanço-Diniz C, & Yamada E (2009). Number and distribution of neurons in the retinal ganglion cell layer in relation to foraging behaviors of tyrant flycatchers. Journal of Comparative Neurology, 514(1):66–73. [PubMed: 19260061]

Coimbra J, Nolan P, Collin S, & Hart N (2012). Retinal ganglion cell topography and spatial resolving power in penguins. Brain, Behavior and Evolution, 80(4):254–68. doi: 10.1159/000341901.

Coimbra J, Hart N, Collin S, & Manger P (2013). Scene from above: retinal ganglion cell topography and spatiall resolving power in the giraffe (Giraffa camelopardalis). Journal of Comparative Neurology, 521(9):2042–57. doi: 10.1002/cne.23271. [PubMed: 23595815]

Cruz-Martín A, El-Danaf R, Osakada F, Sriram B, Dhande O, Nguyen P, Callaway E, Ghosh A, & Huberman A (2014). A dedicated circuit links direction-selective retinal ganglion cells to the primary visual cortex. Nature, 507(7492):358–61. [PubMed: 24572358]

Dacey D (1993). The mosaic of midget ganglion cells in the human retina. Journal of Neuroscience, 13(12):5334–55. [PubMed: 8254378]

Dacey D, & Petersen M (1992). Dendritic field size and morphology of midget and parasol ganglion cells of the human retina. Proceedings of the National Academy of Sciences, 89(20):9666–70.

Davis F (1929). The Anatomy and Histology of the Eye and Orbit of the Rabbit. Transactions of the American Ophthalmological Society, 27:4002–441.

Della Santina L, Inman D, Lupien C, Horner P, & Wong R (2013). Differential progression of structural and functional alterations in distinct retinal ganglion cell types in a mouse model of glaucoma. Journal of Neuroscience, 33(44):17444–57. [PubMed: 24174678]

Dhande O, Estevez M, Quattrochi L, El-Danaf R, Nguyen P, Berson D, & Huberman A(2013) Genetic dissection of retinal inputs to brainstem nuclei controlling image stabilization. Journal of Neuroscience, 33(45):17797–813. [PubMed: 24198370]

Dhande O, Stafford B, Lim J, & Huberman A (2015). Contributions of Retinal Ganglion Cells to Subcortical Visual Processing and Behaviors. Annual Review of Vision Science, 1: 291–328.

Dräger U, & Olsen J (1981). Ganglion cell distribution in the retina of the mouse. Investigative Ophthalmology and Vision Science, 20(3):285–93.

El-Danaf R, &Huberman A (2015). Characteristic patterns of dendritic remodeling in earlystage glaucoma: evidence from genetically identified retinal ganglion cell types. Journal of Neuroscience, 35(6):2329–43. [PubMed: 25673829]

Fite K, & Lister B (1981). Bifoveal vision in anolis lizards. Brain Behavior and Evolution, 19(3–4): 144–54.

Gomes F, Silveira L, Saito C, &Yamada E (2005). Density, proportion, and dendritic coverage of retinal ganglion cells of the common marmoset (Callithrix jacchus jacchus). Brazilian Journal of Medical and Biologiacal Research, 38(6):915–24.

Hayes B, Martin G, & Brooke, Mde L (1991). Novel area serving binocular vision in the retinae of procellariiform seabirds. Brain Behavior and Evolution, 37(2):79–84.

Huberman A, Manu M, Koch S, Susman M, Lutz A, Ullian E, Baccus S, & Barres B (2008). Architecture and activity-mediated refinement of axonal projections from a mosaic of genetically identified retinal ganglion cells. Neuron, 59(3):425–38. [PubMed: 18701068]

Huberman A, Wei W, Elstrott J, Stafford B, Feller M, & Barres B (2009). **Genetic** identification of an On-Off direction-selective retinal ganglion cell subtype reveals a layer-specific subcortical map of posterior motion. Neuron, 62(3):327–34. [PubMed: 19447089]

Huberman A, & Niell C (2011). What can mice tell us about how vision works? Trends Neuroscience, 34(9):464–73.

Hughes S, Watson T, Foster R, Peirson S, & Hankins M (2013). Nonuniform distribution and spectral tuning of photosensitive retinal ganglion cells of the mouse retina. Current Biology, 23(17):1696–701. [PubMed: 23954426]

Inzunza O, Bravo H, Smith R, & Angel M (1991). Topography and morphology of retinal ganglion cells in Falconiforms: a study on predatory and carrion-eating birds. The Anatomical Record, 229(2):271–7. [PubMed: 2012314]

Jakobs T, Libby R, Ben Y, John S, & Masland R (2005). Retinal ganglion cell degeneration is topological but not cell type specific in DBA/2J mice. The Journal of Cell Biology, 171(2):313–25. [PubMed: 16247030]

Jeon C, Strettoi E, & Masland R (1998). The major cell populations of the mouse retina. Journal of Neuroscience, 18(21):8936–46. [PubMed: 9786999]

Jindal V (2015). Interconnection between brain and retinal neurodegenerations. Molecular Neurobiology, 51(3):885–92. [PubMed: 24826919]

Kim I, Zhang Y, Meister M, & Sanes J (2010). Laminar restriction of retinal ganglion cell dendrites and axons: subtype-specific developmental patterns revealed with transgenic markers. Journal of Neuroscience, 30(4):1452–62. [PubMed: 20107072]

Kitazawa Y, & Yamamoto T (1997). Glaucomatous visual field defects: their characteristics and how to detect them. Clinical Neuroscience, 4(5):279–83. [PubMed: 9292256]

Lisney T, & Collin S (2008). Retinal ganglion cell distribution and spatial resolving power in elasmobranchs. Brain Behavior and Evolution, 72(1):59–77. doi: 10.1159/000146082.

Marshel J, Garrett M, Nauhaus I, & Callaway E (2011). Functional specialization of seven mouse visual cortical areas. Neuron, 72(6):1040–54. doi: 10.1016/j.neuron.2011.12.004. [PubMed: 22196338]

Mowat F, Petersen-Jones S, Williamson H, Williams D, Luthert P, Ali R, & Bainbridge J (2008). Topographical characterization of cone photoreceptors and the area centralis of the canine retina. Molecular Vision, 4:2518–27.

Müller P, Müller S, Gliem M, Küpper K, Holz F, Harmening W, Charbel Issa P (2016). Perception of Haidinger Brushes in Macular Disease Depends on Macular Pigment Density and Visual Acuity. Investigative Ophthalmology and Visual Science, 57(3):1448–56. doi: 10.1167/iovs.15-19004. [PubMed: 27028066]

Osterhout J, Josten N, Yamada J, Pan F, Wu S, Nguyen P, Panagiotakos G, Inoue YU, Egusa S, Volgyi B, Inoue T, Bloomfield S, Barres B, Berson D, Feldheim D, & Huberman A (2011). Cadherin-6 mediates axon-target matching in a non-image-forming visual circuit. Neuron, 71(4):632–9. [PubMed: 21867880]

Osterhout J, El-Danaf R, Nguyen P, & Huberman A (2014). Birthdate and outgrowth timing predict cellular mechanisms of axon target matching in the developing visual pathway. Cell Reports, 8(4): 1006–17. [PubMed: 25088424]

Ou Y, Jo R, Ullian E, Wong R, & Della Santina L (2016). Selective Vulnerability of Specific Retinal Ganglion Cell Types and Synapses after Transient Ocular Hypertension. Journal of Neuroscience, 36(35):9240–52. [PubMed: 27581463]

Oyster C, Takahashi E, & Hurst D (1981). Density, soma size, and regional distribution of rabbit retinal ganglion cells. Journal of Neuroscience, 1(12):1331–46. [PubMed: 7320749]

Peichl L (1992). Topography of ganglion cells in the dog and wolf retina. Journal of Comparative Neurology, 324(4):603–20. [PubMed: 1385496]

Pettigrew J, Bhagwandin A, Haagensen M, & Manger P (2010). Visual acuity and heterogeneities of retinal ganglion cell densities and the tapetum lucidum of the African elephant (Loxodonta africana). Brain Behavior and Evolution, 75(4):251–61. doi: 10.1159/000314898.

Rivlin-Etzion M, Zhou K, Wei W, Elstrott J, Nguyen P, Barres B, Huberman A, & Feller M (2011). Transgenic mice reveal unexpected diversity of on-off direction-selective retinal ganglion cell subtypes and brain structures involved in motion processing. Journal of Neuroscience, 31(24): 8760–9. [PubMed: 21677160]

Seabrook T, Burbridge T, Crair M, & Huberman A (2017). Architecture, Function and Assembly of the mouse visual system. Annual Reviews of Neurocience, 40: in press.

Stafford B, Park S, Wong K, & Demb J (2014). Developmental changes in NMDA receptor subunit composition at ON and OFF bipolar cell synapses onto direction-selective retinal ganglion cells. Journal of Neuroscience, 34(5):1942–8. [PubMed: 24478373]

Stewart W, & Shields M (1991). The peripheral visual field in glaucoma: reevaluation in the age of automated perimetry. Survey of Ophthalmology, 36(1):59–69. [PubMed: 1925946]

Stone J, & Halasz P (1989). Topography of the retina in the elephant Loxodonta africana. Brain Behavior and Evolution, 34(2):84–95.

Stone J (1983). Parallel Processing in the Visual System. Boston, MA: Springer.

Sun W, Li N, & He S (2002). Large-scale morphological survey of mouse retinal ganglion cells. Journal of Comparatiave Neurology, 451(2):115–26.

Tootell R, Switkes E, Silverman M, & Hamilton S (1988). Functional anatomy of macaque striate cortex. II. Retinotopic organization. Journal of Neuroscience, 8(5):1531–68. [PubMed: 3367210]

Yamada E, Silveira L, Gomes F & Lee B (1996). The retinal ganglion cell classes of New World primates. Revista Brasileira de Biologia, 56 (Suppl 1): 381–396. [PubMed: 9394516]

Yilmaz M, & Meister M (2013). Rapid innate defensive responses of mice to looming visual stimuli. Current Biology, 23(20):2011–5. doi: 10.1016/j.cub.2013.08.015. [PubMed: 24120636]

Wei W, Elstrott J, & Feller M (2010). Two-photon targeted recording of GFP-expressing neurons for light responses and live-cell imaging in the mouse retina. Nature Protocols, 5(7):1347–52. [PubMed: 20595962]

Wei P, Liu N, Zhang Z, Liu X, Tang Y, He X, Wu B, Zhou Z, Liu Y, Li J, Zhang Y, Zhou X, Xu L, Chen L, Bi G, Hu X, Xu F, & Wang L (2015). Processing of visually evoked innate fear by a non-canonical thalamic pathway. Nature Communications, 6:6756.

Zhang Y, Kim I, Sanes J, & Meister M (2012). The most numerous ganglion cell type of the mouse retina is a selective feature detector. Proceedings of the National Academy of Sciences, 109(36):E2391–8.

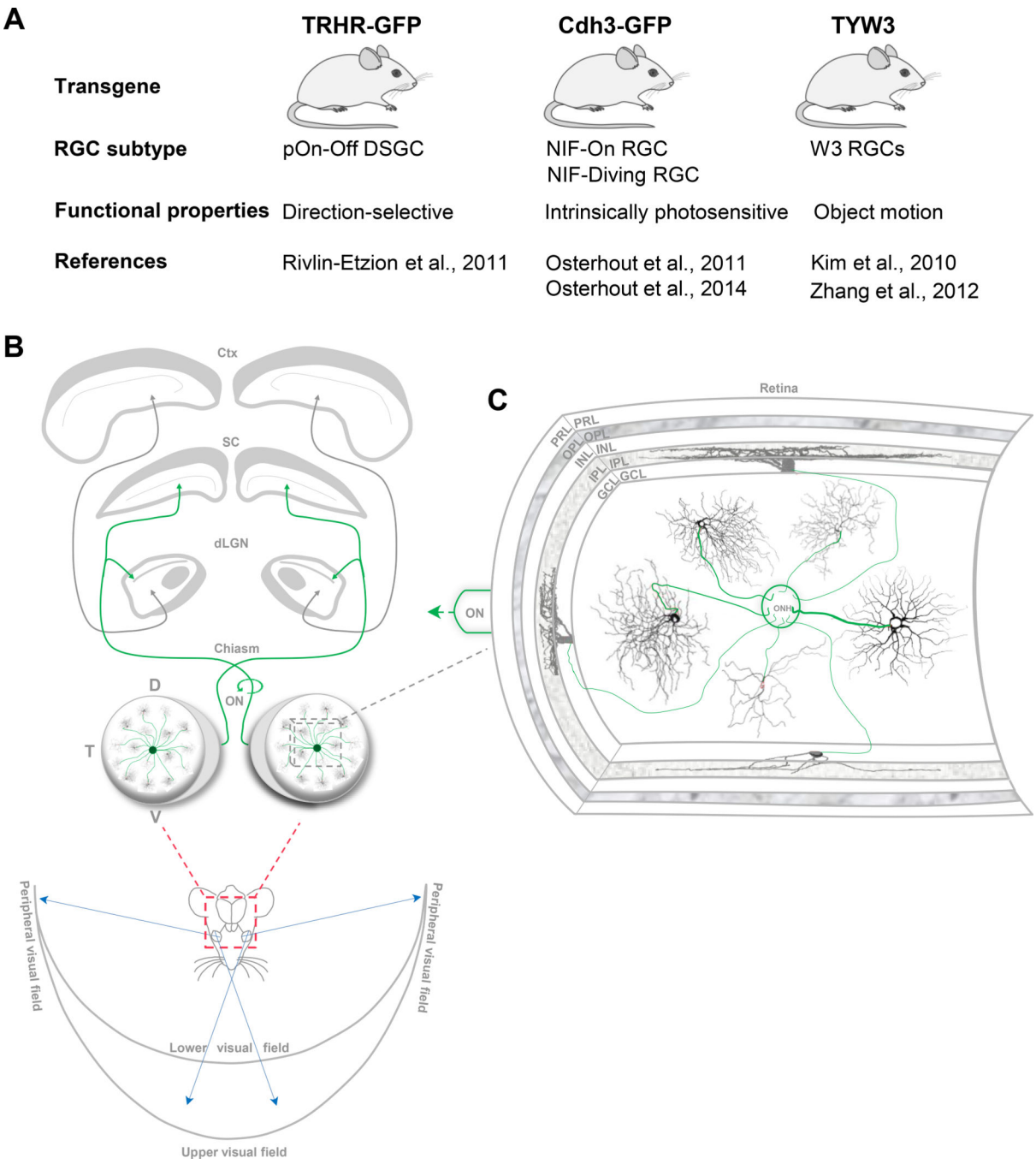

Figure 1.

RGCs provide the link between the eyes and the brain. (A), Summary of the different transgenic mouse lines used in this study along with the corresponding transgenically-labelled RGCs subtypes. (B), All information from various points in visual space enter the eyes where it's converted into neuronal signals and relayed to center brain nuclei. RGCs in both eyes are positioned at various retinal locations, transmit visual information to various nuclei in the brain via the optic nerve (ON) (Green, RGC axons). D, dorsal; N, nasal; T, temporal; V, ventral; dLGN, dorsal lateral geniculate nucleus; SC, superior colliculus; ctx,

cortex. (C), Inset in (***B***), an illustration (modified from Stone, 1983) showing a cross section of the retina depicting its different layers: PRL, photoreceptor layer; OPL, outer plexiform layer; INL, inner nuclear layer; IPL, inner plexiform layer; GCL, ganglion cell layer. RGCs provide the sole output neurons of the retina by means of their axons (green) forming the ON. RGCs' receive various aspects of visual information via their dendritic arbors, which differ in their *en face* morphologies and stratification patterns in the IPL. ONH, optic nerve head.

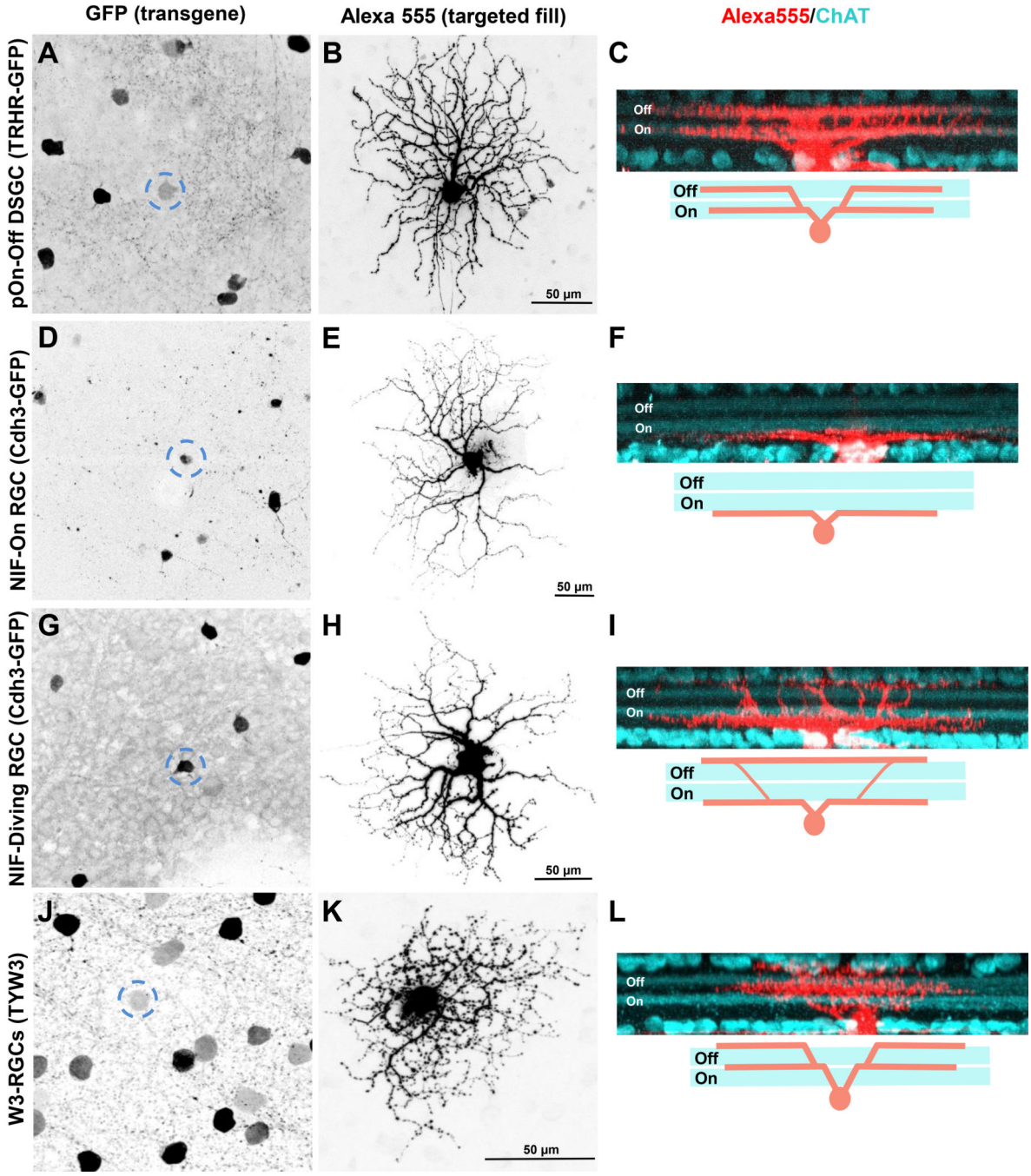

Figure 2.

Specific RGC subtypes are labelled in different transgenic mouse lines. (A-O), Maximum intensity projection images showing GFP^+ (A,D,G) and YFP^+ (J) somas that were targeted with Alexa Fluor 555 to reveal their complete *en face* morphologies (B,E,H,K) and dendritic stratification depth patterns (C,F,I,L; red, cell fill; cyan, ChAT immunostaining) in 3 transgenic mouse lines: TRHR-GFP (A-C: pOn-Off DSGC), Cdh3-GFP (D-F: NIH-On RGC; G-I: NIH-diving RGC) and TYW3 (J-L: W3-RGC). Dashed circles in (A,D,G,J) delineate fluorescently labeled somas that were targeted and filled. Scale, 50 µm. Schematics

underneath (C,F,I,L) represent the distinct dendritic stratification patterns of each RGC subtype.

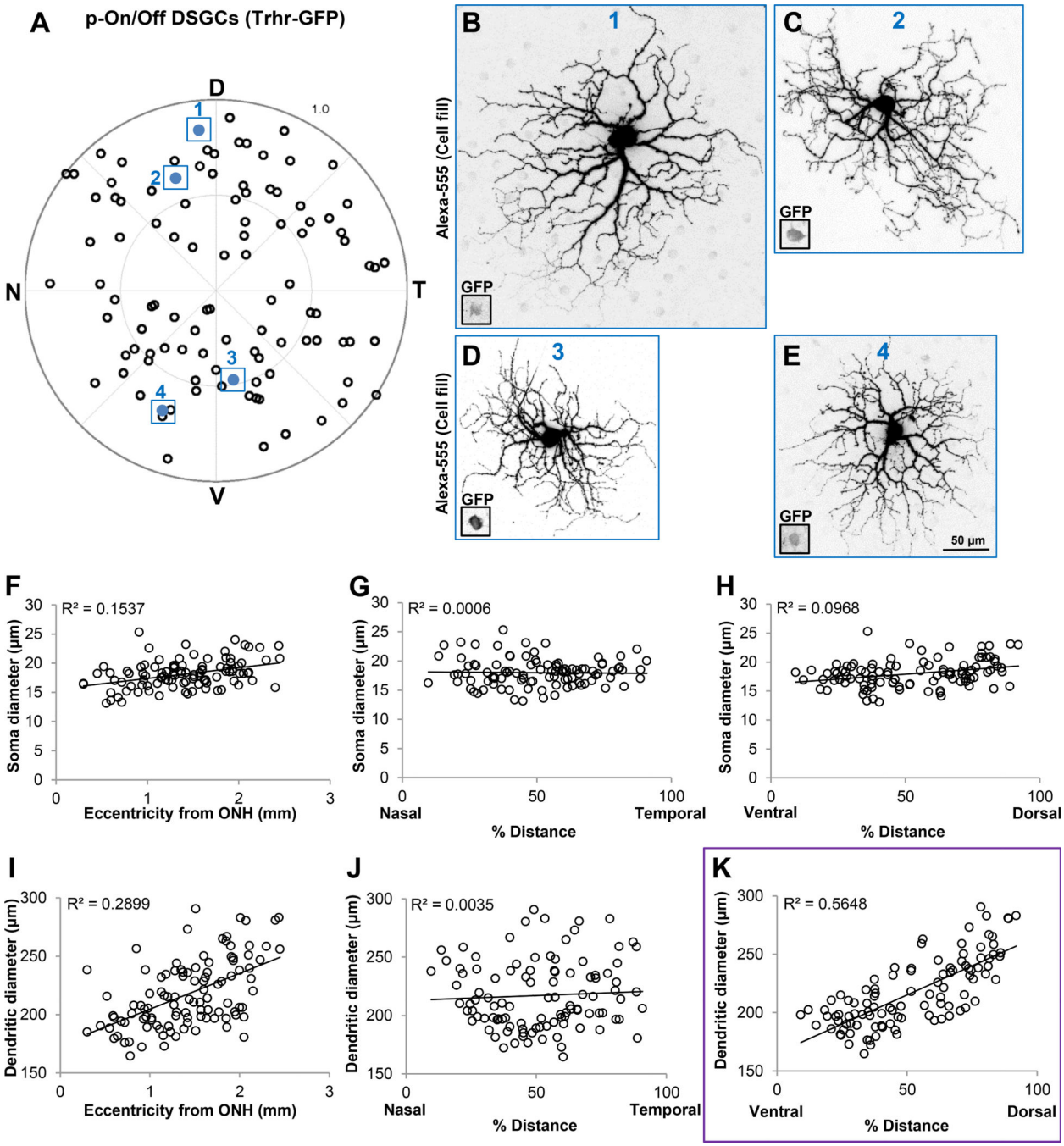

Figure 3.

Dendrites of dorsally located pOn-Off DSGCs are significantly larger than those located in the ventral retina. (A) Polar plot showing the retinal position of each individually filled RGC. D, dorsal; N, nasal; T, temporal; V, ventral. (B-E) Maximum intensity projection images showing dendritic size differences of pOn-Off DSGCs targeted at different retinal locations. All images are shown to scale (50µm) and correspond to cells outlined and colored in (A) (B, cell 1; C, cell 2; D, cell 3; E, cell 4). Insets in (B-E) represent GFP+ somas. (F-H) Scatter plots showing no correlation between soma size and eccentricity (F), %

distance along the N-T axis (G) and % distance along the V-D axis (H). I-K, Scatter plots showing that dendritic diameter size is significantly correlated with RGCs' position along the D-V axis (K, $r^2 = 0.5648$) compared to eccentricity (I) and position along the N-T axis (J). Purple outline in (K***)*** highlights the statistical significance, which can also be seen in examples (B-E). Each dot in (A) and (F-K***)*** represents a single RGC ($n = 105$ RGCs, $N = 16$ mice).

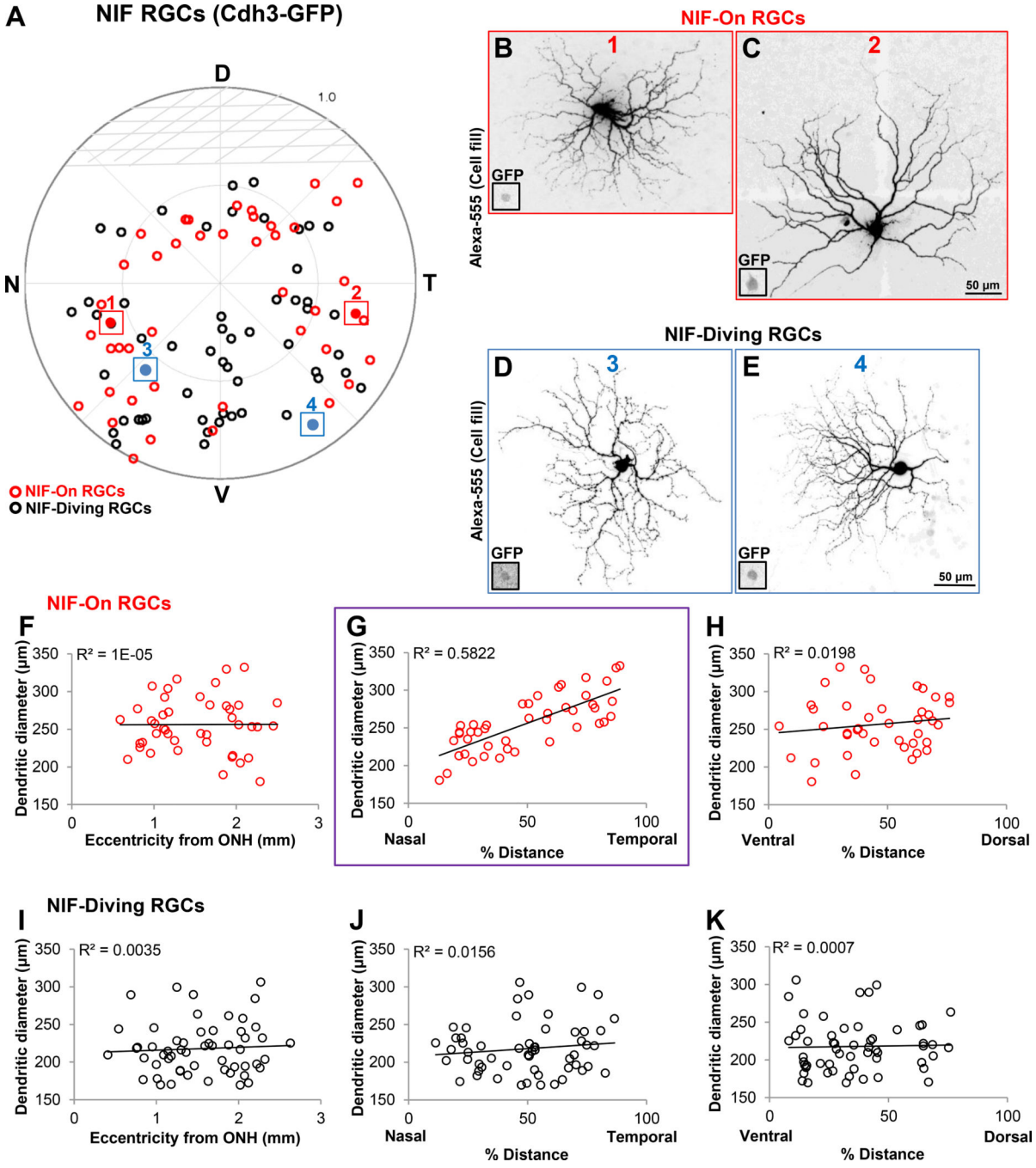

Figure 4.

NIF-On RGCs show a N-T pattern in dendritic size. (A) polar plot showing the retinal location of GFP+ RGCs in the Cdh3-GFP transgenic mouse line (red, NIF-On RGCs; black, NIF-diving RGCs; $n = 100$ RGCs; $N = 10$ mice). Note that there are no RGCs filled in the top dorsal half of the retina, which is consistent with the GFP expression pattern in this transgenic mouse line (Osterhout et al., 2011). D, dorsal; N, nasal; T, temporal; V, ventral. (B-C) Example images of NIF-On RGCs targeted at different locations (B, cell 1 outlined in A; C, cell 2 outlined and colored in A). Scale in (C) corresponds to (B-C), 50 µm. D-E,

Examples showing the morphologies of NIF-diving RGCs obtained from different retinal position where (D) and (E) corresponds to colored cells 3 and 4, respectively. Scale bar in (E) is for (D-E***)***, 50 μm. Insets in (B-E***)*** represent the GFP+ soma of each RGCs depicted. (F-K) Scatter plots showing the relationship between dendritic diameter of NIF-ON RGCs (F-H, $n = 44$) and NIF-diving RGCs (I-K, $n = 56$) as a function of location in the retina. This shows that dendritic diameter of NIF-On RGCs is significantly correlated with position along the N-T axis (G, purple outline, $r^2 = 0.5822$) also apparent in examples (B-C).

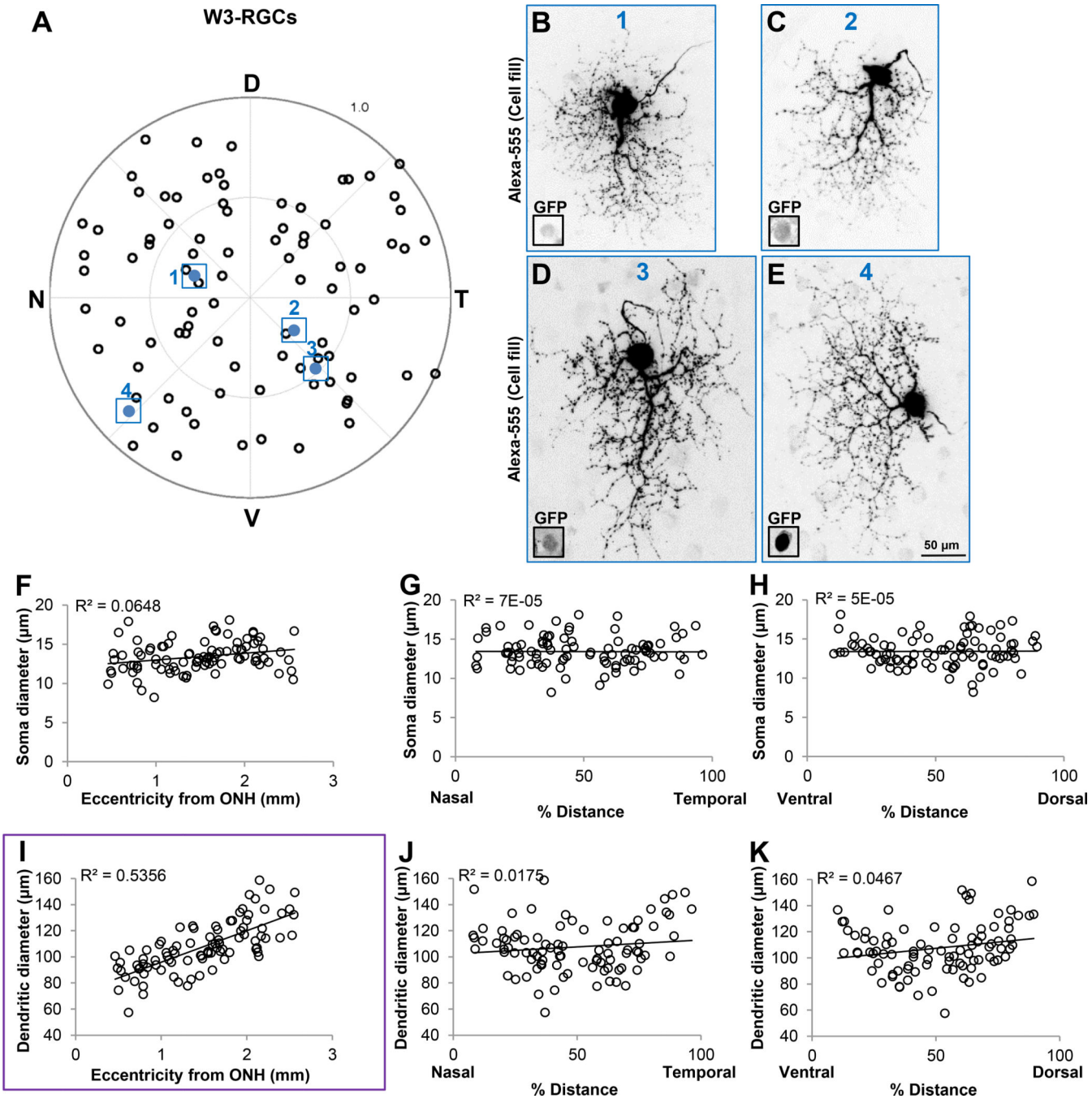

Figure 5.

W3 RGCs' dendrites display eccentricity related changes. (A) Polar plot showing the location of individually filled W3-RGCs in the TYW3 transgenic mouse line (n = 91 RGCs; N = 13 mice). D, dorsal; N, nasal; T, temporal; V, ventral. (B-E) Examples of W3-RGCs targeted in diverse locations showing differences in dendritic field diameter. RGCs in (B-E) correspond to colored cells 1–4 in (A), respectively. Scale in (E) is for (B-E), 50µm. F-H, Scatter plots depicting no significant correlation between soma diameter as a function of eccentricity from ONH (F), % distance along the N-T axis (G) and % distance along the V-D

axis (H). (I-K) Scatter plots showing that dendritic diameter of W3-RGCs is significantly correlated with eccentricity from ONH (I, purple outline, linear regression, $r^2 = 0.5356$) while no correlation exists with % distance along the N-T axis (J) or % distance along the D-V axis (K).

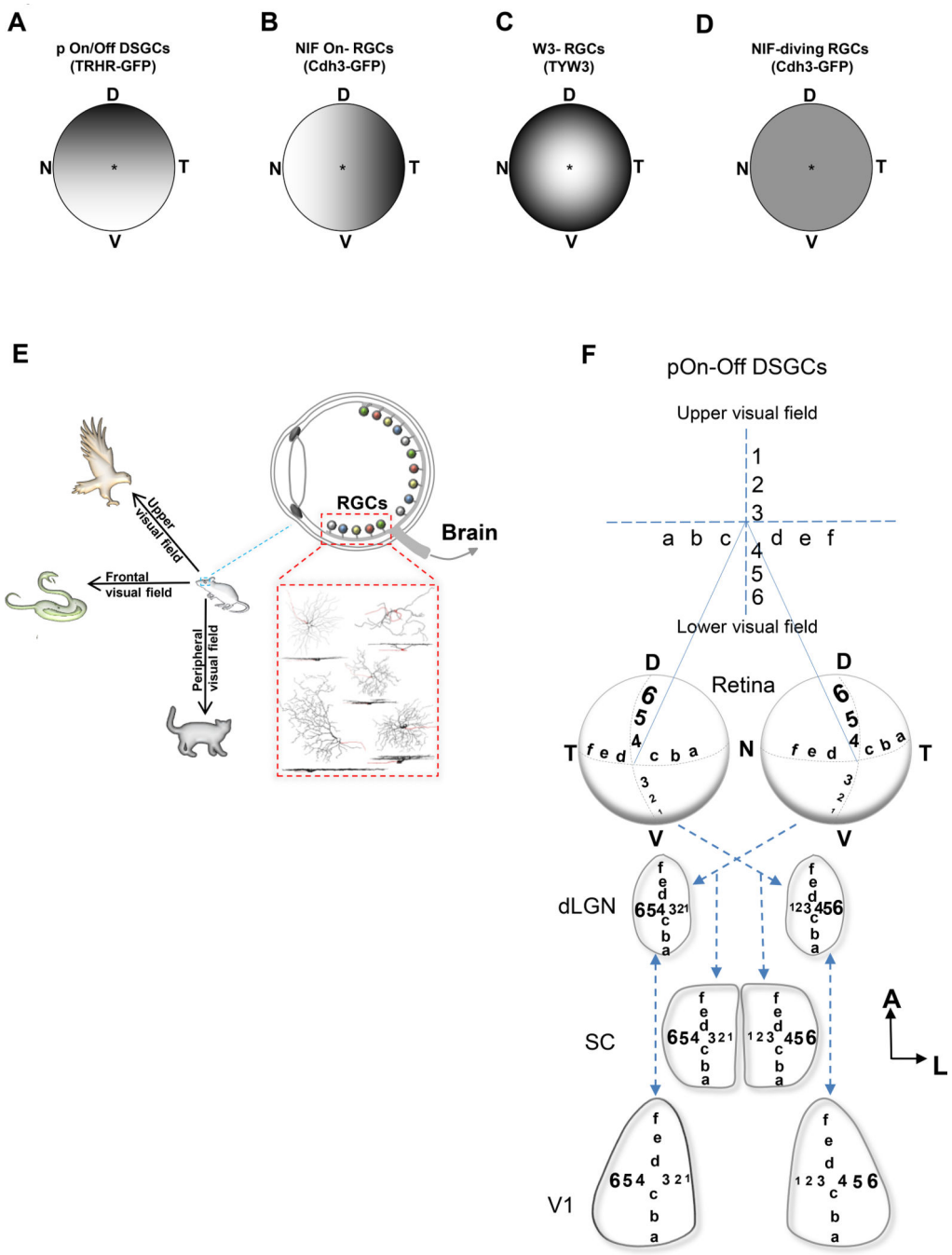

Figure 6.

Mouse retina contains sub-topographical maps for visual signal processing. (A-D) Summary diagrams showing the distributions of dendritic field sizes as a function of retinal location for pOn/Off DSGCs (A), NIF On-RGCs (B), W3-RGCs (C), NIF diving-RGCs (D). (D) dorsal; N, nasal; T, temporal; V, ventral. E, Illustration showing how the distribution of these different RGCs might play a role in their function, and how they are important in dictating survival behaviors in mice.